Latin American Journal of Solids and Structures
www.lajss.org

Modelling of Rocking and Sliding Effects in the Seismic Analysis of a Free-Standing Column

Abstract

A study on the seismic response of a free-standing marble column, including rocking and sliding effects, is presented in this paper. The rocking-sliding model implemented for the development of the analyses corresponds to the basic theoretical and numerical simulation of the dynamic phenomenon. The assessment procedure adopted for the application of the model to the non-linear dynamic incremental time-history investigation is checked by comparison with simplified rigid body-based analytical predictions of the rocking-onset response acceleration and the overturning critical velocity. The results show a high seismic vulnerability of the column, as identified by severe damage at the basic design earthquake level, and an overturning-related near-collapse response at the maximum considered earthquake level.

Keywords

Free-standing columns, rocking, sliding, finite element models, seismic analysis.

S. Sorace [a, *]
G. Terenzi [b]
C. Bitossi [b]
E. Mori [b]

[a] Polythecnic Department of Engineering and Architecture, University of Udine, Via delle Scienze 206, 33100 Udine, Italy
stefano.sorace@uniud.it
[b] Department of Civil and Environmental Engineering, University of Florence, Via S. Marta 3, 50139 Florence, Italy
gloria.terenzi@unifi.it
camilla.bitossi@yahoo.it
elenaemme@virgilio.it

* Corresponding author

http://dx.doi.org/10.1590/1679-78253541

Received 20.11.2016
In revised form 27.02.2017
Accepted 02.03.2017
Available online 04.03.2017

1 INTRODUCTION

The most recent earthquakes that hit heritage sites and museum collections worldwide showed once again the high seismic vulnerability of art objects, as demonstrated by extensive and often irreparable damage, and even complete collapse of a large number of precious assets. Among the various classes of existing artworks, free-standing columns, steles, cabinets and showcases are among the most critical elements, since they are often slender enough to undergo overturning.

The dynamic response of these artefacts is normally amplified by rocking and sliding, even under moderate earthquakes. This imposes to carefully simulate these effects in the finite element analyses supporting the seismic evaluation of any type of free-standing artwork.

A study on this topic is reported in this paper, where a semicircular marble column is selected as representative example. The response of the column is examined according to the seismic assessment procedure proposed in (Sorace and Terenzi, 2007; 2015) for any type of art object, articulated on a set of four seismic performance levels expressly formulated to the purpose, and namely: 1) Rest, 2) No rocking, 3) Damage control/Cultural value safety and 4) Collapse prevention.

A special rocking-sliding finite element model is implemented for the development of the time-history seismic analyses, which corresponds to the basic theoretical and numerical simulation of the dynamic phenomenon. Within this model, rocking is simulated by means of a set of vertical "gap" (no-tension) interface elements linking the joints of the bottom section of the pedestal to the ground, and sliding by plan horizontal friction sliders linking the same joints as the gap elements.

The location layout, geometrical and mechanical characteristics of the examined column, details of the finite element model and a summary of the numerical investigation results are offered in the following sections.

2 CASE STUDY COLUMN: CHARACTERISTICS, MODEL, ANALYSIS AND RESULTS

2.1 Location Layout, Earthquake Levels and Input Ground Motions

The case study column is to be placed, for the development of restoration works, in the joined Laboratories of Stones and Bronzes of the world-famous Opificio delle Pietre Dure (OPD) Institute in Florence. As is known, it is one of the most important art restoration centers worldwide, divided in several special departments dedicated to any type of artworks, each one including diagnostic, intervention, research and teaching activities, and a Museum where selected restored masterpieces of various ages are currently housed.

A drawing of the ground floor plan of the Institute is displayed in Figure 1, where the L-shaped wing of the Laboratories of Stones and Bronzes is highlighted by a hatched background and a continuous-line perimeter contour. The case study artwork will be located in this wing, which is the late 19^{th} century addition of the block, and is constituted by a one-story building, whose façade is shown in Figure 1 too.

The building contains the biggest plants, mobile equipments and artefacts, as well as the widest stocks of materials for the development of the restoration activities of the OPD Institute. As a consequence, the possible earthquake-induced overturning or structural collapse of the most vulnerable art objects and equipments can cause severe damage to several adjacent assets and equipments, as well as seriously affect the safety of the personnel and the visitors.

The seismic performance evaluation enquiry was carried out for the four reference earthquake levels established by current Italian Standards, that is, Frequent Design Earthquake (FDE, with 81% probability of being exceeded over the reference time period V_R); Serviceability Design Earthquake (SDE, with $63\%/V_R$ probability); Basic Design Earthquake (BDE, with $10\%/V_R$ probability); and Maximum Considered Earthquake (MCE, with $5\%/V_R$ probability). The V_R period is fixed at 50 years, which is obtained by multiplying the nominal structural life V_N of 50 years by a

coefficient of use c_u equal to 1. The latter value is adopted because the class of use of the building of the Laboratories is type II (i.e. ordinary), as it can be accessed only by a small number of visitors, in addition to the personnel. By referring to topographic category (TC) equal to T1 (flat surface), and C-type soil (deep deposits of dense or medium-dense sand, gravel or stiff clay from several ten to several hundred meters thick), the peak ground accelerations for the four seismic levels are as follows: 0.071 g (FDE), 0.085 g (SDE), 0.197 g (BDE), and 0.244 g (MCE), with g=acceleration of gravity. The input accelerograms were generated by SIMQKE-II software (Vanmarcke et al., 1999) in families of seven, both for the horizontal and vertical components of seismic action, from the pseudo-acceleration response spectra at linear viscous damping ratio ξ=5% prescribed by the Italian Standards for Florence city, plotted in Figure 2.

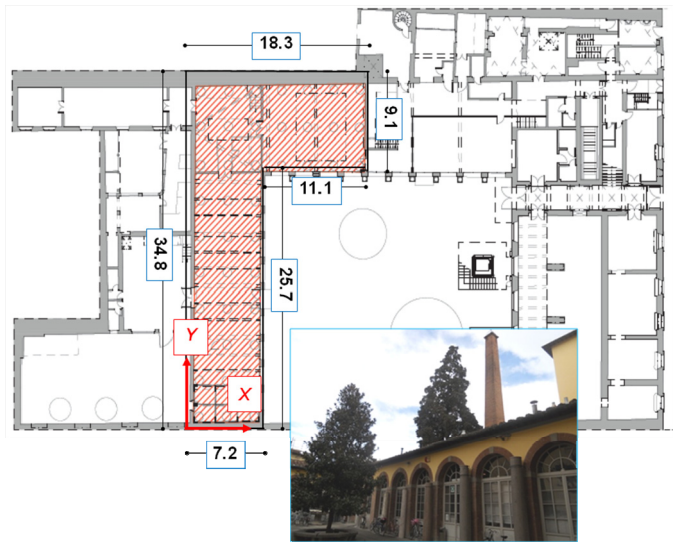

Figure 1: Plan of the ground floor of OPD Institute, with the main hall of the Laboratories of Stones and Bronzes highlighted by a hatched background (dimensions in meters), and view of the building façade.

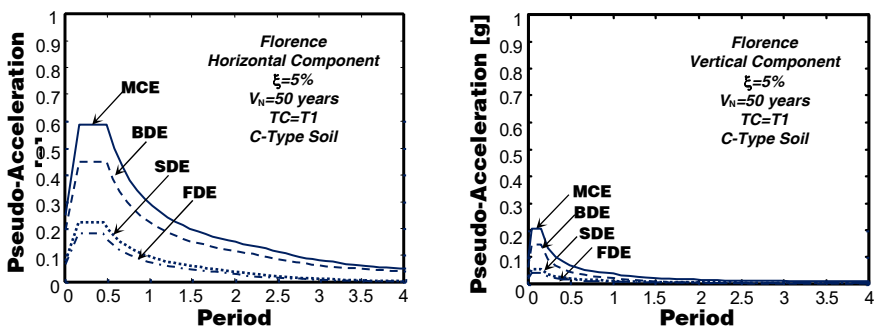

Figure 2: Normative pseudo-acceleration elastic response spectra for the horizontal and vertical earthquake components – Florence city. FDE, SDE, BDE and MCE levels.

2.2 Characteristics of the Column

The case study column is a sculpted monobloc marble element shaped as a semicircular drum, with a multilayer toroidal ring at the bottom and no capital on top, and a parallelepiped pedestal, as illustrated in the drawing of Figure 3. The dimensions of the pedestal in plan are A=724 mm × B=450 mm. The heights of pedestal, multilayer ring and drum are 750 mm, 312 mm and 2085 mm, respectively, for a total height H of 3147 mm.

The constituting material is cipolin marble, traditionally used for ornamental elements, such as floors, coverings, cornices, balustrades and stand-alone columns, like the examined one, rather than as main construction material for structural systems. As no mechanical characterization tests were carried out on the material, its properties were established by referring to the ranges of variation suggested for this type of marble in the literature (Malesani and Vannucci, 1974; Scesi et al., 2006), and namely: uniaxial compressive strength f_{cm}=40–60 MPa; uniaxial tensile strength f_{tm}=0.5–0.8 MPa; Young modulus E_m=20,000–40,000 MPa; Poisson coefficient ν_μ=0.28–0.32; specific weight γ_m=25–27 kN/m^3. In consideration of the absence of direct diagnostic tests, as well as of the ageing and creep-related strength decay occurring throughout the structural life of marbles and stones, the lower limits of the strength ranges above, i.e. f_{cm}=40 MPa and f_{tm}=0.5 MPa, were assumed in the analysis. Concerning E_m, ν_m and γ_m, the mean values of relevant ranges were selected, i.e. E_m=30,000 MPa, ν_m=0.3 and γ_m=26 kN/m^3.

2.3 Modelling of Rocking and Sliding Effects

Unlike the geometrically complex marble statue examined in (Sorace and Terenzi, 2007; 2015), where a smeared-crack numerical model was adopted to detect the evolution of cracking-related damage in the most stressed portions of the mesh, the simple shape and structural configuration of the examined column allowed limiting its assessment analysis to the elastic field. Indeed, these characteristics help easily locate the most critical zones where crack can arise and grow at the foot of the drum, checked by comparing the maximum computed tensile stress values with the corresponding strength f_{tm}.

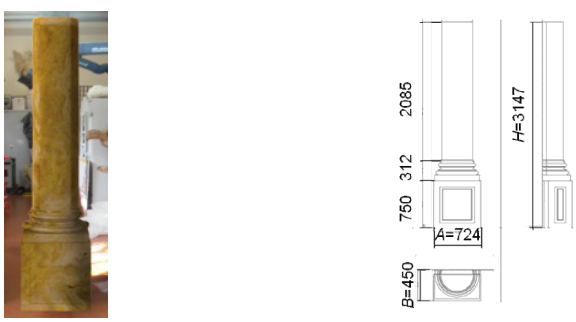

Figure 3: View and geometrical dimensions (in millimetres) of the column.

A 3-D view of the finite element model of the column, generated by SAP2000NL commercial software (CSI, 2016), and the (x_c, y_c, z_c) local reference coordinate system adopted for the genera-

tion of the model are displayed in the image on the left in Figure 4. The mesh is made of 8-node isoparametric solid-type elements with parallelepiped shape, for the pedestal, and prismatic shape, for the drum and the bottom ring. The position of the centre of mass, G, is shown in the drawing on the right in Figure 4, where h_G=1190 mm is the height of G from the base section and b_G=150 mm is the distance of the vertical projection of G from the nearest side of the base section in plan.

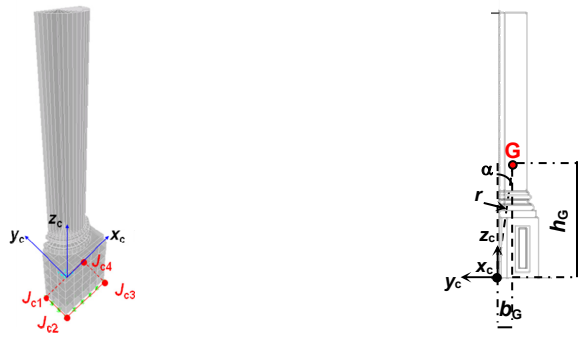

Figure 4: Finite element model of the column and position of the centre of mass.

A rocking-sliding model corresponding to the basic analytical and numerical simulation of the dynamic phenomenon (Shenton and Jones, 1991; Makris and Cameron, 2001; Caliò and Marletta, 2003; Borri and Grazini, 2006; Sorace and Terenzi, 2007; Baratta and Corbi, 2012; Chatzis and Smyth, 2012; Voyagaki et al. 2013) was implemented for the development of the time-history analyses. As detailed in Figure 5, within this model rocking is simulated by means of a set of vertical "gap" (no-tension) interface elements linking the joints of the bottom section of the pedestal to the ground. On the other hand, sliding is reproduced by plan horizontal friction sliders linking the same joints as the gap elements (Figure 6). The sliding friction coefficient between marble and the cotto-tile surface of the floor, μ_c, was fixed at 0.3, i.e. the mean value of the 0.25–0.35 reference range suggested in the literature (Gordon, 1976; ASTM, 2011) for the sliding contact of the two materials.

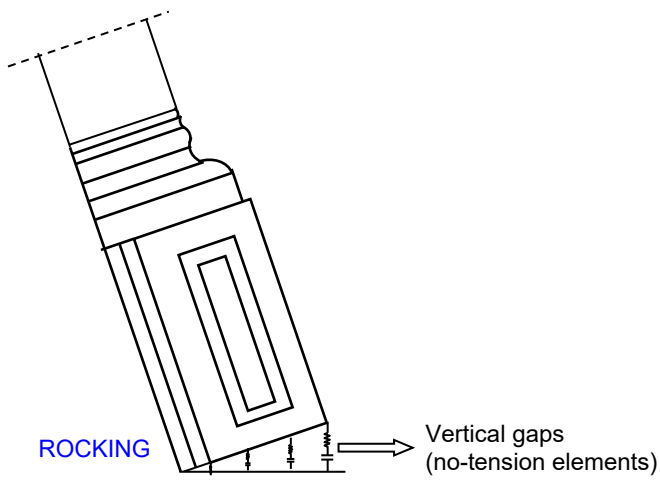

Figure 5: Finite element assembly for the simulation of rocking.

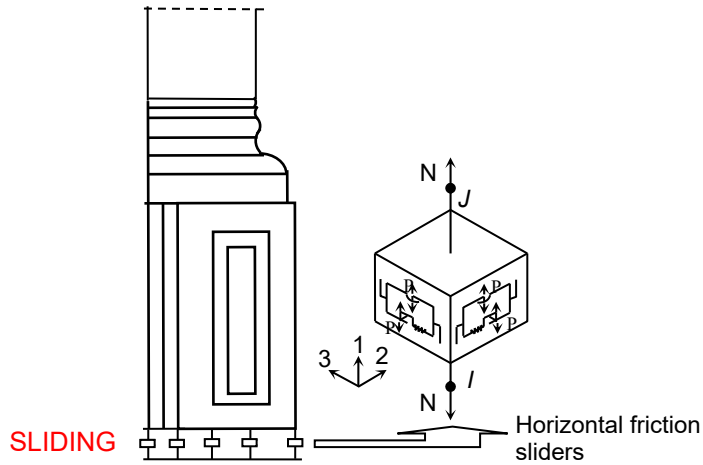

Figure 6: Finite element assembly for the simulation of sliding.

At a first level of approximation, the boundary of No rocking PL for a slender art object like the examined column can be identified with the necessary physical condition for a vertical oscillation around a perimeter side of the base section of the object, considered as a rigid body. Said m and a_t the mass and the absolute acceleration of the column, this condition is reached when the seismically induced moment, M_s, determined by the resultant of the horizontal inertia forces, F_W, applied in G: $M_s=F_W \cdot h_G=m \cdot a_t \cdot h_G$, equals the available resisting moment, M_r, due to gravity: $M_r=P \cdot \delta=m \cdot g \cdot \delta$, where P, g and δ are the own weight of the column, the acceleration of gravity and the horizontal displacement of G, respectively, as schematized in the drawing on the left in Figure 7. Considering that the nearest side of the base section in plan also represents the axis of rotation — relative to the ground — for the considered oscillation plan (y_c–z_c, x_c being the weak flexural axis), the condition above occurs for $\delta=b_G$. The corresponding "critical" (i.e. rocking-onset) response acceleration, a_{cr}, is

$$a_{cr}=\frac{b_G}{h_G} \cdot g \tag{1}$$

By applying Eq. 1 for b_G=150 mm and h_G=1190 mm, a_{cr}=0.126 g is obtained. It should be noted that this a_{cr} estimate, in addition to the assumed rigid body simplified hypothesis, also neglects the effects of the upward earthquake component, as well as of the interaction of rocking with sliding. Therefore, as observed above, this value is only a first equilibrium-based approximation of the rocking-onset acceleration, which can be regarded as a useful comparative term for the time-history results.

In order to identify an actual rocking dynamic response regime from the latter, the minimum number of uplifts of two opposite sides in plan, n_u, and their amplitude, d_v, must be preventively fixed. Based on the results of computational studies carried out at a first stage of this research on several types of artworks, including slender objects, the following values were suggested (Sorace and Terenzi, 2007): 5, for n_u, and 0.5 mm, for d_v. In particular, the d_v limit represents a threshold beyond which uplifts proved to be substantially insensitive to the choice of the most influencing pa-

rameters on the finite element simulation of rocking, i.e. the elastic compression stiffness of the vertical gap elements, the number of gaps linking the base section to the substrate, and the interaction with sliding. At the same time, n_{ul}=5 is a minimal value separating an alternate rocking regime of uplifts from sporadic detachments from the ground with amplitude greater than d_v, regardless of the specific characteristics of the input ground motions (whether of near or far-fault type, natural or artificially generated, amplitude-scaled or not, etc). Consistently with these data, n_{ul}=5 and d_v=0.5 mm were assumed as a reference also for the analysis of the case study column.

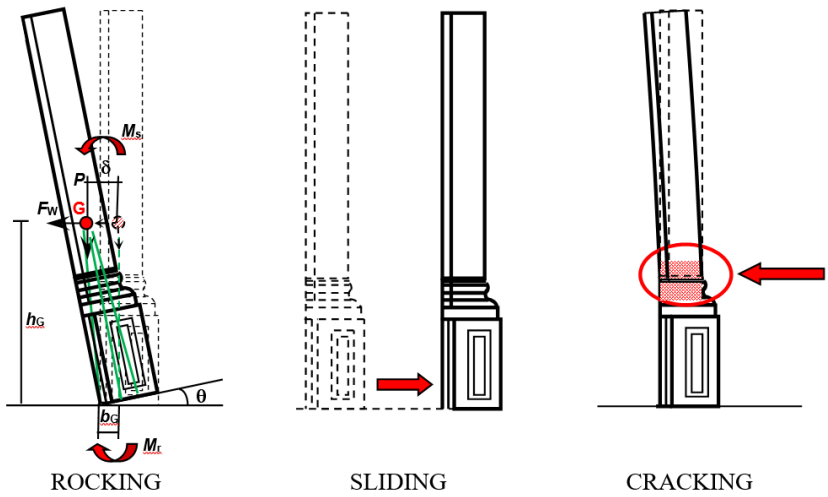

Figure 7: Schematic representation of rocking and sliding at the pedestal-floor interface, and cracking effects in the lower portion of the drum.

As regards the limit conditions of Collapse prevention level, supplementary criteria must be adopted to identify the overturning-related threshold for slender objects. In the rigid-body hypothesis, the classical mixed acceleration–velocity criterion proposed by Ishiyama (1982) can be assumed, for which the lower acceleration limit is given by a_{cr}, whereas the lowest velocity capable of overturning the rocking body, v_{ov}, is approximately expressed as follows:

$$v_{ov} = 0.4\sqrt{\frac{2g}{r}\left(i^2 + r^2\right)\frac{1-cos\alpha}{cos^2\alpha}} \tag{2}$$

where i is the radius of gyration of the body about G, r is the distance from the base edge to G, and α is the angle between the reference vertical axis and the segment joining the base edge to G ($\alpha = arctg\left(b_G / h_G\right)$), in rest conditions. For the case study column r and α are indicated in the image on the right in Figure 4.

For a rectangular body, $i^2 + r^2 = \frac{4}{3}r^2$, in which case Eq. 2 becomes:

$$v_{ov} = 0.4\sqrt{\frac{8g \cdot r}{3} \cdot \frac{1-cos\alpha}{cos^2\alpha}} \tag{3}$$

In order to apply Eq. 3 when the body is not rectangular and also non-symmetric in the main oscillation plan, but it is divided in geometrically regular portions and thus the position of the centre of mass can be precisely calculated (as is the case of the examined column), it can be idealized as an equivalent rectangular block with base equal to $2b_G$, as shown in Figure 8. This schematization was numerically validated in (Boroschek and Romo, 2004) for a wide variety of non-symmetric bodies, as well as of input ground motions, and further checked experimentally in (Boroschek and Iruretagoyena, 2006).

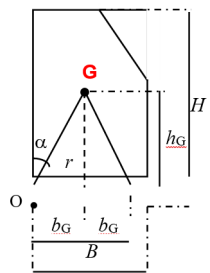

Figure 8: Schematic representation of the geometrical characteristics of a non-symmetric body.

2.4 Results

The overturning velocity calculated by means of Eq. 3 for the equivalent base width $2b_G$=300 mm of the column in the y_c–z_c plan is equal to v_{ov}=202 mm/s, being r=1199.5 mm and α=7.18°.

The vertical displacement histories obtained from the most demanding among the seven groups of input accelerograms are plotted in Figure 9 for the four normative earthquake levels. The graphs are referred to the edge joints of the most distant side of the base section from the vertical projection of G, denoted with symbols J_{c2} and J_{c3} in the finite element model view of Figure 4. The graphs show several small uplifts for the FDE and SDE-scaled actions, with peak values slightly greater than 0.2 mm (FDE) and 0.3 mm (SDE), both neatly below the assumed 0.5 mm rocking-onset threshold, highlighted by a horizontal segment in these diagrams. These response histories identify the decompression of a portion of the base section, assessing that the Rest performance level is exceeded, and the response consequently falls in the No rocking range. At the same time, these data corroborate the first-level evaluation based on the comparison of a_{cr}=0.126 g with the above-mentioned peak ground accelerations for the FDE and SDE, equal to 0.071 g and 0.085 g. Indeed, both values are lower than a_{cr}, practically in the same proportion between the peak uplifts and the 0.5 mm limit, thus prefiguring the No rocking response conditions confirmed by the results of the time-history analyses.

The maximum vertical displacements reach 3.7 mm and 4.8 mm at the BDE and MCE, respectively, which are about 7 and 9 times greater than the rocking-onset limit, repeatedly exceeded during the response. The peak values of the time-history uplifts of the edge joints of the opposite side in plan (J_{c1}, J_{c4} according to the nomenclature in Figure 4), not presented here for brevity's sake, are about half the values found for J_{c2}, J_{c3}. This fraction is well correlated with the ratio of the distances of the two sides from the vertical projection of G, $b_G/(B\text{-}b_G)$=150/(300-150)=0.5.

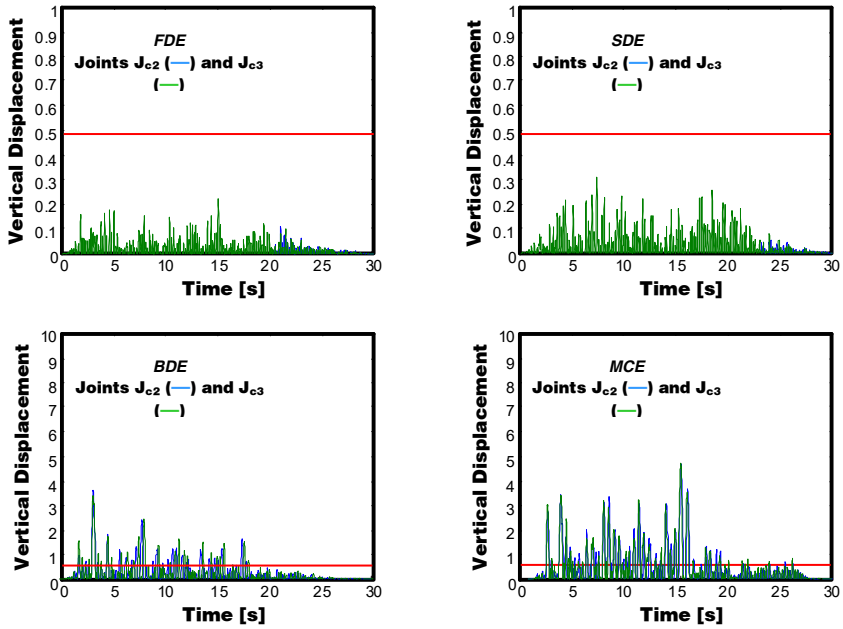

Figure 9: Vertical displacement time-histories of joints Jc2 and Jc3 of the column pedestal.

By summing up the results of the performance assessment analysis, in addition to the FDE–No rocking and SDE–No rocking correlations commented above, BDE–Collapse prevention and MCE–Collapse prevention correlations are found, with small overturning collapse-related safety margins for the MCE.

Additional information on the column performance is derived from the sliding response. As highlighted by the horizontal displacement time-histories of the base section computed for the BDE and MCE, peaks of 4 mm (BDE) and 6 mm (MCE) are obtained. These values are high enough to cause possible pounding conditions should the column be leaning against other artworks or a wall during the restoration works, instead of about at the center of the Laboratories. Furthermore, the response histories of the two joints notably differ at both earthquake levels, and are also divergent at the MCE, highlighting remarkable torsional effects due to asymmetry of the column in the y_c–z_c plan, as well as to the combined action of the earthquake components along axes x_c and y_c.

In order to evaluate whether the activation of this pronounced rocking regime also corresponds to the attainment of the Damage Control limits, the vertical tensile stress envelopes obtained at the BDE and MCE for the same groups of input accelerograms are reproduced in Figure 10. As expected, the most stressed portion of the mesh is situated at the base of the drum and across the underlying multi-layer ring zone, marked by an ellipse in the drawing on the right in Figure 7 and by circles in the finite element model views of Figure 10. The peak tensile stress values, surveyed in the rear side of the second ring from the bottom, characterized by the smallest cross section, are equal to 0.58 MPa (BDE) and 0.77 MPa (MCE), that is about 15% and 50% greater than f_t. This underlines that cracks might already open in this ring at the BDE, thus exceeding the limit conditions of Damage control/Cultural value safety PL, and significantly spread to the other rings and the base section of the drum at the MCE. The peak ground velocity for the BDE and MCE is equal

to 145.6 mm/s and 183.8 mm/s, respectively. By comparing these values with the v_{ov} estimate of 202 mm/s, near-overturning conditions are assessed for the highest earthquake level. Indeed, the difference between the MCE-related peak velocity and v_{ov}, lower than 10%, represents a small safety margin, in consideration of the inherent approximations involved in v_{ov} calculation.

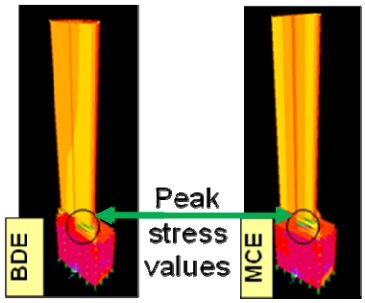

Figure 10: Vertical tensile normal stress contours in the column model at the BDE (left) and MCE.

2.5 Observations on Mount Making Strategies

The results of the seismic analysis carried out on the examined column, representative of a wide class of overturning-prone slender free-standing artworks, underline that proper technical prevention measures should be adopted. A mount making strategy sometimes implemented in permanent exhibitions consist in fixing the objects tightly to the base, which also allows removing any possible rocking and tilting effects from their dynamic response (Lowry et al., 2007). However, although meeting the desired stability requirements, base-fixing strategies imply that the seismic accelerations occurring at the base of the objects are fully transmitted to them. This causes severe damages at the BDE and MCE levels, even leading to strength-related (instead of overturning-induced) collapses, especially in artworks made of low tensile strength materials (Borri and Grazini, 2006; Sorace and Terenzi, 2015). An effective alternative installation strategy, increasingly investigated and applied during the last decade, is represented by seismic isolation, either of single objects (Contento and Di Egidio, 2009; Vassiliou and Makris, 2012; Chiozzi et al., 2016) or of groups of artefacts placed on the same floor (Sorace and Terenzi, 2015). The merit of these advanced installation solutions is that a very high protection level is guaranteed to any type of art objects, independently of their specific material, mechanical and geometric characteristics.

3 CONCLUSIONS

The finite element analyses carried out on the case study column allowed evaluating the influence of rocking and sliding on its dynamic response, as well as assessing its remarkable vulnerability under seismic action scaled at the two highest normative earthquake levels.

The activation of a pronounced mixed rocking-sliding response regime is noticed in the column beginning from the Basic Design Earthquake (BDE) level of seismic action, causing the attainment of the Damage control/Cultural value safety limits, with the opening of cracks in the bottom portion of the artefact.

At the same time, overturning conditions are assessed for the Maximum Considered Earthquake (MCE) by comparing the dynamic rocking response of the column with the overturning-related limit condition for slender objects expressed by the classical Ishiyama mixed acceleration–velocity criterion. As a consequence, the Collapse prevention condition is not met at the highest normative level of seismic action.

Aknowledgements

The study reported in this paper was sponsored by the Italian Department of Civil Protection within the ReLUIS-DPC Project 2014/2018 – Research programme Nr. 6: Isolation and Dissipation. The authors gratefully acknowledge this financial support.

References

ASTM D2047-11 (2011). Standard test method for static coefficient of friction of polish-coated flooring surfaces as measured by the James machine, ASTM – American Society for Testing and Materials International, West Conshohocken, PA.

Baratta, A., Corbi, O. (2012). Analysis of the dynamics of rigid blocks using the theory of distributions. Advances in Engineering Software 44: 15–25.

Boroschek, R., Iruretagoyena, A. (2006). Controlled overturning of unanchored rigid bodies. Earthquake Engineering & Structural Dynamics 35: 695–711.

Boroschek, R., Romo, D. (2004). Overturning criteria for non-anchored non-symmetric rigid bodies. In: Proc. of the 13th WCEE, Vancouver, Canada, Paper No. 295.

Borri, A., Grazini, A. (2006). Diagnostic analysis of the lesions and stability of Michelangelo's David. Journal of Cultural Heritage 7: 273–285.

Caliò, I., Marletta, M. (2003). Passive control of the seismic rocking response of art objects. Engineering Structures 25: 1009–1018.

Callister, W.D. (1999). Material science and engineering: an introduction, fifth ed., John Wiley & Sons Inc., New York, NY.

Chatzis, M., Smyth, A. (2012). Robust Modeling of the Rocking Problem. Journal of Engineering Mechanics 138: 247–262.

Chiozzi, A., Simoni, M., Tralli, A. (2016). Base isolation of heavy non-structural monolithic objects at the top of a masonry monumental construction. Materials and Structures 49: 2113–2130.

Contento, A., Di Egidio, A. (2009). Investigations into benefits of base isolation for non-symmetric rigid blocks. Earthquake Engineering and Structural Dynamics 38: 849–866.

CSI (2016). SAP2000NL. Theoretical and users' manual. Release 17.08. Computers & Structures Inc, Berkeley, CA.

Gordon, J.E. (1976). The Science of structures and materials. Scientific American Library, New York, NY.

Ishiyama, Y. (1982). Motion of rigid bodies and criteria for overturning by earthquake excitations. Earthquake Engineering & Structural Dynamics 10: 630–650.

Lowry, M.K., Farrar, B.J., Armendariz, D., Podany, J. (2007). Protecting collections in the J. Paul Getty Museum from earthquake damage. WAAC Newsletter 29: 16–23.

Makris, N., Cameron, C.J. (2001). Rocking response of equipment anchored to a base foundation. Pacific Earthquake Engineering Research Center, Berkeley, CA.

Malesani, P.P., Vannucci, S.A. (1974). Research on degradation of stones. Leo Olschky, Florence, Italy.

Scesi, L., Papini, M., Gattinoni, P. (2006). Geologia applicata: il rilevamento geologico tecnico. Ed. Ambrosiana, Milan, Italy [in Italian].

Shenton, H.W., Jones, N.P. (1991). Base excitation of rigid bodies. II: Periodic slide-rock response. J. Engineering Mechanics ASCE 117: 2307–2328.

Sorace, S. and Terenzi, G. (2007). Rebuilding of an ancient castle including a base-isolated museum hall. In: Structural Studies, Repairs and Maintenance of Heritage Architecture X. WIT Transactions on the Built Environment, WIT Press, Southampton, UK: 419-428.

Sorace, S. and Terenzi, G. (2015). Seismic performance assessment and base isolated floor-protection of statues exhibited in museum halls. Bulletin of Earthquake Engineering 13: 1873-1892.

Tucker, M.E. (2001). Sedimentary petrology. An introduction to the origin of sedimentary rocks, third ed., Blackwell Science, Oxford, UK.

Vanmarcke, E.H., Fenton, G.A., Heredia-Zavoni, E. (1999). SIMQKE-II – Conditioned earthquake ground motion simulator: User's manual, Version 2.1, Princeton University, Princeton, NJ. URL http://nisee.berkeley.edu/documents/SW/ SIMQKE-II-V2-1.pdf.

Vassiliou, M.F., Makris, N. (2012). Analysis of the rocking response of rigid blocks standing free on a seismically isolated base. Earthquake Engineering & Structural Dynamics 41: 177–196.

Voyagaki, E., Psycharis, I.N,. Mylonakis, G. (2013). Rocking response and overturning criteria for free standing rigid blocks to single—lobe pulses. Soil Dynamics and Earthquake Engineering 46: 85–95.